Nano Research

ISSN 1998-0124 CN 11-5974/O4
https://doi.org/10.1007/s12274-021-3294-2

Research Article

Semiconducting M_2X (M = Cu, Ag, Au; X = S, Se, Te) monolayers: A broad range of band gaps and high carrier mobilities

Lei Gao[1,2], Yan-Fang Zhang[1], and Shixuan Du[1,3] (✉)

[1] *Institute of Physics & University of Chinese Academy of Sciences, Chinese Academy of Sciences, Beijing 100190, China*
[2] *Faculty of Science, Kunming University of Science and Technology, Kunming 650000, China*
[3] *CAS Key Laboratory of Vacuum Physics, Beijing 100049, China*

Received: 10 October 2020 / **Revised:** 9 December 2020 / **Accepted:** 13 December 2020

ABSTRACT

Two-dimensional semiconductors (2DSCs) with appropriate band gaps and high mobilities are highly desired for future-generation electronic and optoelectronic applications. Here, using first-principles calculations, we report a novel class of 2DSCs, group-11-chalcogenide monolayers (M_2X, M = Cu, Ag, Au; X = S, Se, Te), featuring with a broad range of energy band gaps and high carrier mobilities. Their energy band gaps extend from 0.49 to 3.76 eV at a hybrid density functional level, covering from ultraviolet-A, visible light to near-infrared region, which are crucial for broadband photoresponse. Significantly, the calculated room-temperature carrier mobilities of the M_2X monolayers are as high as thousands of $cm^2 \cdot V^{-1} \cdot s^{-1}$. Particularly, the carrier mobilities of η-Au_2Se and ε-Au_2Te are up to 10^4 $cm^2 \cdot V^{-1} \cdot s^{-1}$, which is very attractive for electronic devices. Benefitting from the broad range of energy band gaps and superior carrier mobilities, the group-11-chalcogenide M_2X monolayers are promising candidates for future-generation nanoelectronics and optoelectronics.

KEYWORDS

two-dimensional semiconductors, group-11-chalcogenides, electronic properties, first-principles calculations

1 Introduction

Two-dimensional semiconductors (2DSCs) have attracted tremendous attention in condensed matter physics and materials research due to their novel and superior transport properties, which may shape future-generation electronic and optoelectronic devices [1–7]. For making high-performance miniaturized devices, such as ultrathin channel field-effect transistors (FETs), 2DSCs with suitable band gaps, high carrier mobilities, and high air-stability are essential [8]. Up to now, 2D transition-metal dichalcogenides (TMDs) and black phosphorus are of wide interest owing to their moderate band gaps. However, 2D TMDs possess relatively low carrier mobility on the order of a few hundreds of $cm^2 \cdot V^{-1} \cdot s^{-1}$ [9]. Though the carrier mobility of 2D black phosphorus has been predicted up to 10^3–10^4 $cm^2 \cdot V^{-1} \cdot s^{-1}$, it is easily oxidized in air, limiting its future application [10, 11]. So, exploring air-stable 2DSCs with suitable band gaps and high carrier mobilities is still highly desired.

Recently, air-stable semiconducting Cu_2Se [12] and Cu_2Te [13] monolayers with six-atom-thick and hexagonal symmetry have been experimentally fabricated on bilayer graphene. Meanwhile, three-atom-thick Cu_2S [14] and Au_2S [15] monolayers with square symmetry have been theoretically predicted to be semiconductors with high carrier mobilitiy and high oxidation resistibility. These experimental and theoretical studies have brought group-11 (Cu, Ag, Au) chalcogenides into the family of 2DSCs as promising candidates for ultrathin channel FET devices, which require air-stable 2DSCs with suitable band gaps and high carrier mobilities. Therefore, group-11-chalcogenide monolayers (M_2X, M = Cu, Ag, Au; X = S, Se, Te) merit further exploration by using theoretical calculations and experiment.

In this paper, based on first-principles calculations, we carried out a systematic investigation of group-11-chalcogenide monolayers (M_2X, M = Cu, Ag, Au; X = S, Se, Te). Among different allotropes of group-11-chalcogenide M_2X monolayers, θ-Cu_2S, ζ-Cu_2Se, ζ-Cu_2Te, η-Ag_2S, η-Ag_2Se, ζ-Ag_2Te, ι-Au_2S, η-Au_2Se, and ε-Au_2Te are not only energetically favorable but also thermodynamically stable. These M_2X monolayers possess energy band gaps ranging from 0.49 to 3.76 eV. The energy levels of conduction band minimum (CBM, −4.94 to −2.65 eV) and valence band maximum (VBM, −6.41 to −4.41 eV) are also in a broad range, which are important in the design of van der Waals heterostructures for optoelectronic applications. Furthuremore, the room-temperature carrier mobilities of the M_2X monolayers are as high as thousands of $cm^2 \cdot V^{-1} \cdot s^{-1}$, while those of η-$Au_2Se$ and ε-Au_2Te are up to 10^4 $cm^2 \cdot V^{-1} \cdot s^{-1}$.

2 Results and discussion

Unlike 2D TMDs, which are naturally layer-stacked in their bulk phase, group-11-chalcogenides are not layered, meaning that the coresponding monolayers can not be obtained from their 3D counterparts. Here, we report a class of possible allotropes of monolayer group-11-chalcogenide (M_2X, M = Cu, Ag, Au; X = S, Se, Te) as shown in Fig. 1, with four hexagonal (α, β, γ, δ), two rectangular (ε, ζ), and three square (η, θ, ι) lattices.

Address correspondence to sxdu@iphy.ac.cn

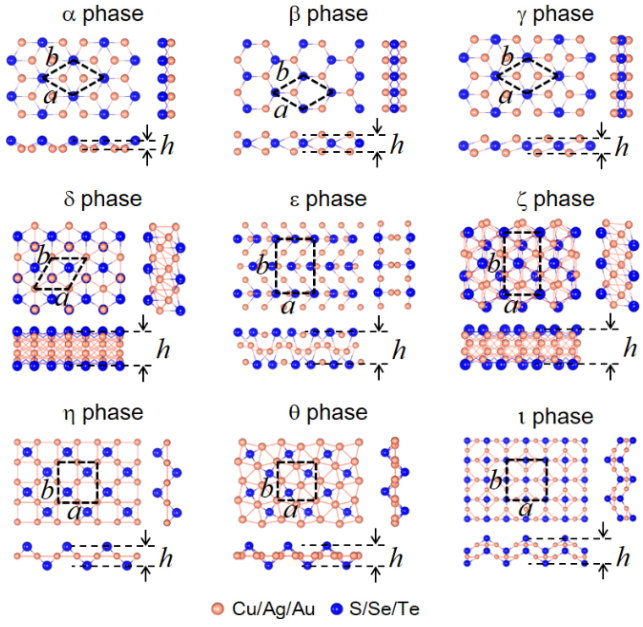

Figure 1 Allotropes of group-11-chalcogenide monolayers (M_2X, M = Cu, Ag, Au; X = S, Se, Te): top views and side views from *x* and *y* horizontal directions with four hexagonal (α, β, γ, δ), two rectangular (ε, ζ), and three square (η, θ, ι) lattices. *a* and *b* are the lattice parameters. *h* is the thickness of M_2X monolayers.

First, we compared the energies of the nine possible monolayer allotropes for each group-11-chalcogenides (M_2X, M = Cu, Ag, Au; X = S, Se, Te), as shown in Fig. 2. Among the nine possible allotropes, the most energetically favorable sturcture is the ζ phase for Cu_2Se, Cu_2Te, and Ag_2Te, while it is the η phase for Ag_2S, Ag_2Se, and Au_2Se. For Cu_2S, Au_2S, and Au_2Te, the lowest-energy configurations are θ-Cu_2S, ι-Au_2S, and ε-Au_2Te, respectively. We noticed that, for the energetically favorable M_2X monolayers, group-11 elements prefer to be sandwiched between chalcogens, which are expected to contribute to excellent oxidation resistance.

To futher investigate the thermodynamic stability of M_2X monolayers, we then performed phonon dispersion calculations. The phonon dispersions of the energetically favorable M_2X monolayers (θ-Cu_2S, ζ-Cu_2Se, ζ-Cu_2Te, η-Ag_2S, η-Ag_2Se, ζ-Ag_2Te, ι-Au_2S, η-Au_2Se, and ε-Au_2Te) and others are shown in Fig. 2 and Fig. S1 in the Electronic Supplementary Material (ESM), respectively. For the energetically favorable M_2X monolayers, there is no appreciable imaginary phonon mode, indicating these M_2X monolayers are dynamically stable. To further check the thermal stabilities of M_2X monolayers, we performed *ab initio* molecular dynamic calculations at 300 K for 2 ps using about 2 nm × 2 nm supercells of M_2X monolayers. As seen in Fig. S2 in the ESM, the integrity of the original configurations with time evolution confirms their good thermal stability. The optimized structure parameters are shown in Table S1 in the ESM. We further summarized the stable/metastable phases of M_2X monolayers in Fig. S3 in the ESM. Although they adopt different stable configurations due to their non-layer bulk phases, there are some regularities of the stable phases of M_2X monolayers. It is symmetric along the diagonal from the top right to the bottom left. From the top to the bottom, it is from Cu, Ag to Au, in which the ability of donating electrons decreases. From the right to the left, it is from Te, Se to S, in which the ability of accepting electrons increases. The ability of donating (accepting) electrons for the cations (anions) is probably related to the formation of different phases, yeiding the symmetric regularity of the stable/metastable phases of M_2X monolayers, which needs more experimental and theoretical investegations to figure out.

The recently fabricated low-temperature (< 147 K) phase monolayer Cu_2Se [12] agrees well with our proposed ζ-Cu_2Se. Considering the rapid development of experimental techniques for fabricating 2D materials in recent years, we are optimistic that other members of these M_2X monolayers can be fabricated experimentally in the near future. Since their non-layer bulk phases, it is suggested that they can be synthesized via molecular

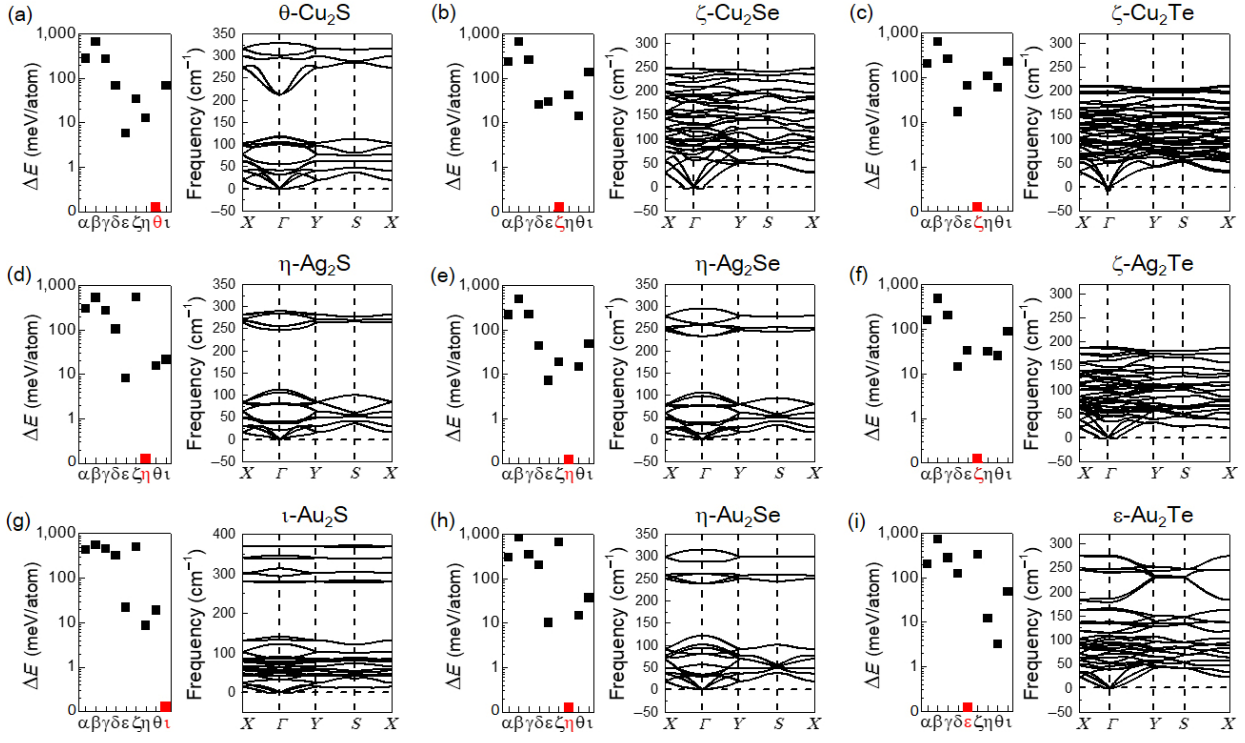

Figure 2 (a)–(i) Relative energies of the nine allotropes and the phonon dispersions of the lowest-energy phase for each M_2X. The allotropes with the lowest energies are marked in red, which are θ-Cu_2S, ζ-Cu_2Se, ζ-Cu_2Te, η-Ag_2S, η-Ag_2Se, ζ-Ag_2Te, ι-Au_2S, η-Au_2Se, and ε-Au_2Te, respectively.

beam epitaxy (MBE) or chemical vapour deposition (CVD) methods, which have been extensively utilized for exploration of new 2D materials [16, 17], such as monolayer Cu_2Se and Cu_2Te [12, 13]. In the following, we further explore the electronic structures of these structural stable M_2X monolayers.

The band structures and band edges of M_2X monolayers have been calculated at the HSE06 level. As shown in Fig. 3, θ-Cu_2S, η-Ag_2S, η-Ag_2Se, ζ-Ag_2Te, and η-Au_2Se are direct band-gap semiconductors with band gaps of 1.10, 2.63, 2.61, 1.26, and 1.61 eV at the Γ point, respectively. ζ-Cu_2Se, ζ-Cu_2Te, ι-Au_2S, and ε-Au_2Te are indirect band-gap semiconductors with band gaps of 1.23, 0.49, 3.76, and 1.27 eV, respectively. Electronic structures of other M_2X monolayers can be found in Fig. S4 in the ESM. Among these metastable M_2X monolayers in different phases, most of them are semiconductors except θ-Au_2Te showing metallic behavior. The band gap values of semiconducting M_2X monolayers extend from 0.49 to 3.76 eV, which correspond to photon wavelengths from 340 to 2,530 nm, covering the ultraviolet-A, visible light, and near-infrared region. Such broad range of energy band gaps is crucial for optical and optoelectronic applications which require broadband photoresponse. Additionally, the optical absorbances of M_2X monolayers are provided in Fig. S5 in the ESM for reference. Among all the materials, ζ-Cu_2Se, ζ-Cu_2Te, ζ-Ag_2Te, and ε-Au_2Te monolayers show relatively high absorbances which are ~ 10%–25% at the visible light region, much higher than those of monolayer t-ZnS [18], BiOI [19], etc., which are smaller than 5%. These M_2X monolayers offer appealing alternative platform for realizing optoelectronic applications.

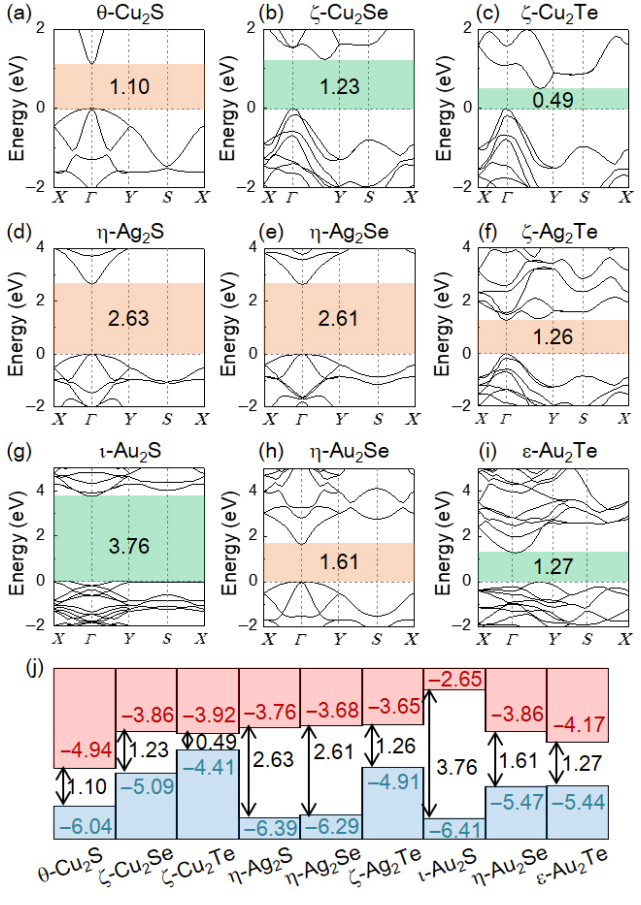

Figure 3 (a)–(i) Band structures of monolayer θ-Cu_2S, ζ-Cu_2Se, ζ-Cu_2Te, η-Ag_2S, η-Ag_2Se, ζ-Ag_2Te, ι-Au_2S, η-Au_2Se, and ε-Au_2Te, respectively. The numbers in each panel indicate the band gaps. The orange and green shaded regions denote direct and indirect band gaps, respectively. (j) CBM and VBM positions of M_2X monolayers.

Furthermore, the CBM and VBM energy levels of these M_2X monolayers are also provided in Fig. 3(j). The CBM energy levels of M_2X monolayers are from –4.94 to –2.65 eV, while the energy levels of VBM vary from –6.41 to –4.41 eV. The various CBM and VBM energy levels are very promising for designing heterostructure based electronic and optoelectronic devices.

Besides electronic band gap and CBM/VBM energy levels, carrier mobility also governs the applications of 2DSCs to a large extent. Thus, we next explored the room-temperature carrier mobilities of M_2X monolayers based on the deformation potential theory [20–22],

$$\mu_{2D} = \frac{e\hbar^3 C_{2D}}{k_B T m^* m_d (E_l)^2} \quad (1)$$

where e, $\hbar$, and k_B are the electron charge, reduced Planck constant, and Boltzmann constant, respectively. The temperature T is set to be 300 K. The carrier mobilities of M_2X monolayers are determined by effective mass m^* ($m_d = \sqrt{m_x^* m_y^*}$, average effective mass), deformation potential E_l, and 2D elastic modulus C_{2D}, which are summarized in Table S2 in the ESM.

Most of the M_2X monolayers hold moderately large room-temperature carrier mobilities, as shown in Fig. 4 (thousands of $cm^2 \cdot V^{-1} \cdot s^{-1}$). We compared them with experimentally/theoretically (dark/ light gray) reported mobilities of single-layer transition-metal dichalcogenide (s-TMD), black phosphorus (BP), and graphene [23, 24]. Of particular interest is that η-Au_2Se and ε-Au_2Te have high mobilities up to 10^4 $cm^2 \cdot V^{-1} \cdot s^{-1}$, comparable to black phosphorus. η-Au_2Se is isotropic, while ε-Au_2Te is anisotropic. Similar to the high-mobility transport anisotroy of black phosphorus, the electron mobility of ε-Au_2Te along y direction is nearly a hundredfold higher than that along x direction, 11,040–14,850 $cm^2 \cdot V^{-1} \cdot s^{-1}$ versus 130–140 $cm^2 \cdot V^{-1} \cdot s^{-1}$. Moreover, the photoconductivities of M_2X monolayers are provided in Fig. S6 in the ESM for reference. The photoconductivities of ζ-Cu_2Se, ζ-Cu_2Te, ζ-Ag_2Te, and ε-Au_2Te monolayers are relatively high. Considering these four M_2X monolayers possessing very high stability, relatively good optical absorbance, and photoconductivity, especially the experimental realization of ζ-Cu_2Se, they may have potential application as photocatalysts.

Since spin-orbit coupling (SOC) effect is usually obvious for the compounds containing heavy elements, such as Te, we further investigate the electronic properties of M_2Te (M = Cu, Ag, Au) monolayers with SOC as shown in Fig. S7 in the ESM. The inclusion of SOC effects slightly decreases the band gap of the M_2Te monolayers. In addition, the valence bands split

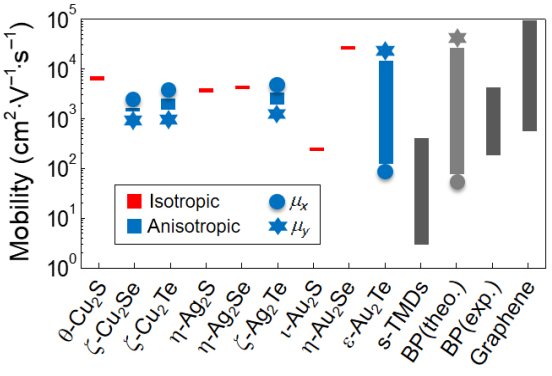

Figure 4 Room-temperature carrier mobilities of M_2X monolayers, compared with experimentally/theoretically (dark/light gray) reported mobilities of single-layer transition-metal dichalcogenide, black phosphorus, and graphene. For anisotropic monolayers ζ-Cu_2Se, ζ-Cu_2Te, ζ-Ag_2Te, and ε-Au_2Te, carrier mobilities along x and y directions are both provided.

around the *S* points due to the SOC effect. However, the band-edge characters around the *Γ* points are nearly the same with and without SOC effects. Considering that the CBMs and VBMs are all located far away from *S* points, it can be concluded that the HSE06 band structures without SOC are able to provide an accurate qualitative picture of the electronic structure in M_2X monolayers in most cases. Figures S7(g) and S7(h) in the ESM present the band-edge energy levels and the carrier mobilities with and without SOC, which are in consistant with the above discussions.

3 Conclusions

In summary, we systematically investegated a family of 2DSCs, group-11-chalcogenide M_2X monolayers, using first-principles calculations. We found that M_2X monolayers adopt different stable configurations due to their non-layer bulk phases. Interestingly, group-11 elements prefer to be sandwiched between chalcogens in the form of monolayers, suggesting excellent oxidation resistance. More importantly, M_2X monolayers exhibit a broad range of band gaps and various CBM/VBM energy levels. Meanwhile, they possess high carrier mobilities of about 10^3–10^4 $cm^2 \cdot V^{-1} \cdot s^{-1}$, which are essential for novel applications in nanoelectronics and optoelectronics. With the rapid development of experimental fabrication techniques, we believe that the predictions on the stable configurations, electronic band structures, and room-temperature carrier mobilities of group-11-chalcogenide M_2X monolayers will inspire experimental researchers to extend 2DSCs to group-11-chalcogenides and some of the predicted M_2X monolayers can be realized in the near future.

4 Methods

First-principles calculations were performed using the Vienna *ab initio* simulation package (VASP) [25, 26]. A generalized gradient approximation (GGA) in the form of Perdew–Burke–Ernzerhof (PBE) [27] is used for the exchange and correlation functional. The screened hybrid functional in the Heyd–Scuseria–Ernzerhof (HSE06) form [28], which can give a better description of band gaps in semiconductors generally, are used to determine the band gaps. The electronic wavefunctions are expanded in a plane wave basis with an energy cutoff of 450 eV. In all the calculations, a 15 Å vacuum layer is used, and all atoms are fully relaxed until the residual forces on each atom are smaller than 10^{-3} $eV \cdot Å^{-1}$. Phonon dispersion is calculated based on a supercell using the finite displacement method as implemented in the PHONOPY package [29–31].

Acknowledgements

This work was financially supported by the National Natural Science Foundation of China (No. 61888102), the National Key Research and Development Projects of China (No. 2016YFA0202300), the Strategic Priority Research Program of the Chinese Academy of Sciences (No. XDB30000000), and the Fundamental Research Funds for the Central Universities.

Electronic Supplementary Material: Supplementary material (molecular dynamic simulations, optical properties, photoelectric properties, structural information and details about carrier mobilities of stable M_2X monolayers, phonon dispersions and band structures of metastable M_2X monolayers) is available in the online version of this article at https://doi.org/10.1007/s12274-021-3294-2.

References

[1] Chhowalla, M.; Jena, D.; Zhang, H. Two-dimensional semiconductors for transistors. *Nat. Rev. Mater.* **2016**, *1*, 16052.
[2] Zeng, M. Q.; Xiao, Y.; Liu, J. X.; Yang, K. N.; Fu, L. Exploring two-dimensional materials toward the next-generation circuits: From monomer design to assembly control. *Chem. Rev.* **2018**, *118*, 6236–6296.
[3] Choi, W.; Choudhary, N.; Han, G. H.; Park, J.; Akinwande, D.; Lee, Y. H. Recent development of two-dimensional transition metal dichalcogenides and their applications. *Mater. Today* **2017**, *20*, 116–130.
[4] Manzeli, S.; Ovchinnikov, D.; Pasquier, D.; Yazyev, O. V.; Kis, A. 2D transition metal dichalcogenides. *Nat. Rev. Mater.* **2017**, *2*, 17033.
[5] Zhang, S. L.; Guo, S. Y.; Chen, Z. F.; Wang, Y. L.; Gao, H. J.; Gó mez-Herrero, J.; Ares, P.; Zamora, F.; Zhu, Z.; Zeng, H. B. Recent progress in 2D group-VA semiconductors: From theory to experiment. *Chem. Soc. Rev.* **2018**, *47*, 982–1021.
[6] Pang, J. B.; Mendes, R. G.; Bachmatiuk, A.; Zhao, L.; Ta, H. Q.; Gemming, T.; Liu, H.; Liu, Z. F.; Rummeli, M. H. Applications of 2D MXenes in energy conversion and storage systems. *Chem. Soc. Rev.* **2019**, *48*, 72–133.
[7] Long, M. S.; Wang, P.; Fang, H. H.; Hu, W. D. Progress, challenges, and opportunities for 2D material based photodetectors. *Adv. Funct. Mater.* **2019**, *29*, 1803807.
[8] Wu, J. X.; Yuan, H. T.; Meng, M. M.; Chen, C.; Sun, Y.; Chen, Z. Y.; Dang, W. H.; Tan, C. W.; Liu, Y. J.; Yin, J. B. et al. High electron mobility and quantum oscillations in non-encapsulated ultrathin semiconducting Bi_2O_2Se. *Nat. Nanotechnol.* **2017**, *12*, 530−534.
[9] Wang, Q. H.; Kalantar-Zadeh, K.; Kis, A.; Coleman, J. N.; Strano, M. S. Electronics and optoelectronics of two-dimensional transition metal dichalcogenides. *Nat. Nanotechnol.* **2012**, *7*, 699–712.
[10] Li, L. K.; Yu, Y. J.; Ye, G. J.; Ge, Q. Q.; Ou, X. D.; Wu, H.; Feng, D. L.; Chen, X. H.; Zhang, Y. B. Black phosphorus field-effect transistors. *Nat. Nanotechnol.* **2014**, *9*, 372−377.
[11] Zhou, Q. H.; Chen, Q.; Tong, Y. L.; Wang, J. L. Light-induced ambient degradation of few-layer black phosphorus: Mechanism and protection. *Angew. Chem., Int. Ed.* **2016**, *55*, 11437−11441.
[12] Qian, K.; Gao, L.; Chen, X. Y.; Li, H.; Zhang, S.; Zhang, X. L.; Zhu, S. Y.; Yan, J. H.; Bao, D. L.; Cao, L. et al. Air-stable monolayer Cu_2Se exhibits a purely thermal structural phase transition. *Adv. Mater.* **2020**, *32*, 1908314.
[13] Qian, K.; Gao, L.; Li, H.; Zhang, S.; Yan, J. H.; Liu, C.; Wang, J. O.; Qian, T.; Ding, H.; Zhang, Y. Y. et al. Epitaxial growth and air-stability of monolayer Cu_2Te. *Chin. Phys. B* **2020**, *29*, 018104.
[14] Guo, Y.; Wu, Q. S.; Li, Y. H.; Lu, N.; Mao, K. K.; Bai, Y. Z.; Zhao, J. J.; Wang, J. L.; Zeng, X. C. Copper(I) sulfide: A two-dimensional semiconductor with superior oxidation resistance and high carrier mobility. *Nanoscale Horiz.* **2019**, *4*, 223–230.
[15] Wu, Q. S.; Xu, W. W.; Lin, D. D.; Wang, J. L.; Zeng, X. C. Two-dimensional gold sulfide monolayers with direct band gap and ultrahigh electron mobility. *J. Phys. Chem. Lett.* **2019**, *10*, 3773–3778.
[16] Cai, Z. Y.; Liu, B. L.; Zou, X. L.; Cheng, H. M. Chemical vapor deposition growth and applications of two-dimensional materials and their heterostructures. *Chem. Rev.* **2018**, *118*, 6091–6133.
[17] Li, G.; Zhang, Y. Y.; Guo, H.; Huang, L.; Lu, H. L.; Lin, X.; Wang, Y. L.; Du, S. X.; Gao, H. J. Epitaxial growth and physical properties of 2D materials beyond graphene: From monatomic materials to binary compounds. *Chem. Soc. Rev.* **2018**, *47*, 6073–6100.
[18] Zhou, J.; Zhen, X. F. A theoretical perspective of the enhanced photocatalytic properties achieved by forming tetragonal ZnS/ZnSe hetero-bilayer. *Phys. Chem. Chem. Phys.* **2018**, *20*, 9950–9956.
[19] Wang, J. J.; Zhang, M.; Meng, J.; Li, Q. X.; Yang, J. L. Single- and few-layer BiOI as promising photocatalysts for solar water splitting. *RSC Adv.* **2017**, *7*, 24446–24452.
[20] Bruzzone, S.; Fiori, G. *Ab-initio* simulations of deformation potentials and electron mobility in chemically modified graphene and two-dimensional hexagonal boron-nitride. *Appl. Phys. Lett.* **2011**, *99*, 222108.
[21] Fiori, G.; Iannaccone, G. Multiscale modeling for graphene-based nanoscale transistors. *Proc. IEEE* **2013**, *101*, 1653–1669.

[22] Takagi, S.; Toriumi, A.; Iwase, M.; Tango, H. On the universality of inversion layer mobility in Si MOSFET's: Part I-effects of substrate impurity concentration. *IEEE Trans. Electr. Dev.* **1994**, *41*, 2357–2362.
[23] Akinwande, D.; Petrone, N.; Hone, J. Two-dimensional flexible nanoelectronics. *Nat. Commun.* **2014**, *5*, 5678.
[24] Qiao, J. S.; Kong, X. H.; Hu, Z. X.; Yang, F.; Ji, W. High-mobility transport anisotropy and linear dichroism in few-layer black phosphorus. *Nat. Commun.* **2014**, *5*, 4475.
[25] Kresse, G.; Furthmüller, J. Efficient iterative schemes for *ab initio* total-energy calculations using a plane-wave basis set. *Phys. Rev. B* **1996**, *54*, 11169.
[26] Kresse, G.; Furthmüller, J. Efficiency of *ab-initio* total energy calculations for metals and semiconductors using a plane-wave basis set. *Comput. Mater. Sci.* **1996**, *6*, 15–50.
[27] Perdew, J. P.; Burke, K.; Ernzerhof, M. Generalized gradient approximation made simple. *Phys. Rev. Lett.* **1996**, *77*, 3865–3868.
[28] Heyd, J.; Scuseria, G. E.; Ernzerhof, M. Hybrid functionals based on a screened Coulomb potential. *J. Chem. Phys.* **2003**, *118*, 8207–8215.
[29] Togo, A.; Oba, F.; Tanaka, I. First-principles calculations of the ferroelastic transition between rutile-type and $CaCl_2$-type SiO_2 at high pressures. *Phys. Rev. B* **2008**, *78*, 134106.
[30] Togo, A.; Tanaka, I. First principles phonon calculations in materials science. *Scr. Mater.* **2015**, *108*, 1–5.
[31] Parlinski, K.; Li, Z. Q.; Kawazoe, Y. First-principles determination of the soft mode in cubic ZrO_2. *Phys. Rev. Lett.* **1997**, *78*, 4063–4066.